metals

MDPI

Article

Aging Phenomena during In-Service Creep Exposure of Heat-Resistant Steels

G. N. Haidemenopoulos [1,2,*], K. Polychronopoulou [1,3], A. D. Zervaki [2], H. Kamoutsi [2], S. I. Alkhoori [1], S. Jaffar [1], P. Cho [1] and H. Mavros [1]

1 Department of Mechanical Engineering, Khalifa University, Abu Dhabi 127788, UAE
2 Department of Mechanical Engineering, University of Thessaly, Volos 38334, Greece
3 Center for Catalysis and Separations, Khalifa University, Abu Dhabi 127788, UAE
* Correspondence: hgreg@mie.uth.gr

Received: 17 June 2019; Accepted: 17 July 2019; Published: 19 July 2019

Abstract: An investigation of aging phenomena during creep exposure has been conducted for HP-Nb cast reformer tubes for several exposure conditions. Aging was manifested by carbide precipitation, carbide coarsening, and carbide transformation. The transformation of primary M_7C_3 to the more stable $M_{23}C_6$ carbide takes place at high exposure temperature (910 °C and above). The primary MC carbides transform to the Ni-Nb silicide or G-phase during creep exposure. The presence of Ti in the steel prevented the transformation of MC carbides to the G-phase. Morphological changes like needle to globular transitions, rounding of carbide edges, and carbide coarsening take place during creep exposure. The room-temperature tensile elongation and ultimate tensile strength are significantly reduced during creep exposure. The above aging phenomena are precursors to creep damage.

Keywords: creep; steam reforming; carbides; G-phase; aging; cast reformer tubes

1. Introduction

Catalytic reforming is routinely employed in oil refineries for the production of petroleum byproducts. The process takes place in tubes suspended in a furnace at a high temperature. The tubes are fed with hydrocarbon, mostly methane, and steam mixture in the presence of a catalyst according to the reaction network:

$$C_nH_m + nH_2O \rightarrow nCO + (\frac{m}{2} + n)H_2, \quad (1)$$

$$CO + H_2O \leftrightarrow CO_2 + H_2. \quad (2)$$

The first is the steam reforming reaction, which, for the case of methane, is strongly endothermic (ΔH_r = 206 KJ/mol) and takes place at a high temperature of the order of 900 °C. The second is the water-gas shift reaction and is mildly exothermic (ΔH_r = −41 KJ/mol). The internal pressure in the tubes generates stresses, causing creep of the tube material. However, prior to creep damage, several aging phenomena take place, which gradually changes the microstructure of the material. The reformer furnace tubes are centrifugally cast and are manufactured from heat-resistant steels, containing Ni and Cr. The current state-of-the-art is to use modified HP-alloys (25Cr-35Ni), with Nb and/or Ti additions. Niobium is added for the precipitation of NbC, which due to its thermal stability contributes to an increased creep resistance [1,2]. Centrifugal casting results in austenitic dendritic grains oriented in the radial direction from the inside diameter (ID) towards the outside diameter (OD) of the tube. The material is strengthened by a network of primary interdendritic carbides. The design life of these tubes is 100,000 h (11.4 years) according to API recommended practice [3]. Premature failures of reformer tubes are frequently observed and are caused by various mechanisms such as creep, carburization, and thermal shock. Evaluation of creep damage in reformer tubes has been

reported by several investigators, either after creep testing [2,4,5], after a certain operational time [6–10], or after premature tube rupture [11,12]. In addition, specific studies of microstructural evolution after long-term aging at high temperatures have been performed [13–15]. The present work contributes to the study of the evolution of carbides and other intermetallic compounds with aging during creep exposure. These phenomena lead to a decrease of ductility and may lead to cracking from thermal stresses during shut-down and start-up operations or during weld repairs.

It is important to note that most of the published data are concerned with studies involving laboratory creep exposure. Results based on specimens taken from real service are rather rare. It is not common to retrieve specimens during a shut-down of a reformer furnace. Therefore, the value of the present work is that the analysis was based entirely on specimens of reformer tubes extracted after a certain operational period, before the end of operational life, and for different temperatures.

2. Materials and Methods

Sections of reformer tubes with an internal diameter of 103 mm and a thickness of 15 mm were retrieved from an oil refinery after 11 years of service. These sections correspond to isothermal operation at three different temperatures 830, 880, and 910 °C and are named as conditions L, M, and H respectively. Another section came from a tube that operated for 8 years at 910 °C and was then nipped for the remaining 3 years, during which the temperature was 950 °C. This section corresponds to condition X. The material of these sections is an HP25Cr-35Ni alloy with Nb addition (HP-Nb steel). The creep strain was estimated by measurements of the outer diameter of the tubes to be of the order of 0.2%. It was also possible to retrieve a section of a reformer tube from another refinery after 5 years of service at 910 °C. This condition is named H5 and the chemical composition of H5 is similar to the previous one with the most important difference being the addition of Ti. This tube sampling enabled the study of the effect of temperature on aging phenomena by comparing sections L, M, H, and X. At the same time, the effect of time and Ti addition could also be performed by comparing sections H and H5. Chemical analysis of the tube materials was performed by optical emission spectrometry. The composition of the alloys and creep exposure conditions are shown in Table 1.

Table 1. Composition (wt%) of the alloys and creep exposure conditions.

Code	T (°C)	t (y)	C	Si	Mn	P	S	Cr	Ni	Nb	Mo	Ti	Fe
L	830	11	0.49	2	0.80	0.01	0.01	25.7	33.6	0.93	0.18	-	B
M	880	11											
H	910	11											
X	910/950	8/3											
H5	910	5	0.41	1.6	1.0	0.02	0.01	24	34.7	0.96	0.07	0.2	B

Characterization of microstructure, including aging phenomena, carbide transformation, and carbide morphology was performed by means of light optical metallography (LOM) and scanning electron microscopy equipped with an energy dispersive X-ray analysis system (EDX). Metallography was performed on thickness specimens from all tube sections. Specimen preparation for metallography involved cutting with a Struers Labotom-3 machine (Struers, Ballerup, Denmark), grinding with SiC papers with 240, 400, 800, 1200, and 2400 grit, polishing with 6, 3, and 1 μm diamond paste and finishing with colloidal silica suspension of 0.04 μm. The etching was performed by swabbing with Kalling's reagent ($CuCl_2$ in a mixture of hydrochloric acid and ethanol). Optical metallography was performed on an Olympus inverted microscope (Olympus, Tokyo, Japan) at magnifications 50–1000×. Scanning electron microscopy (SEM) was performed on etched specimens on a field emission JEOL JSM 7610F (JEOL, Tokyo, Japan) and Quanta 3D microscopes (ThermoFisher Scientific, Hillsboro, OR, USA)equipped with an energy dispersive X-ray analysis (EDX) detector (Oxford Instruments, Abingdon, UK). Imaging was performed with secondary electron mode (SE) and in certain cases

with backscattered electron (BSE) mode. Room temperature uniaxial tensile testing was performed according to ISO 6892 specification [16].

3. Results

3.1. Tensile Properties

Room temperature tensile testing results are shown in Figure 1. The results indicate a decrease of the ultimate tensile strength (UTS) and a considerable reduction in tensile elongation (strain to failure) with exposure temperature, as a result of aging. Condition H5 also exhibits considerable reduction in elongation, however the elongation is higher than the elongation of condition H. Similar reductions in tensile ductility have been reported by Pan et al. [11] after 36,000 h at 910 °C (4.12 years), and Monobe et al. [13] after exposure for 200 h at 720–780 °C. The aging phenomena and carbide transformations are discussed in the following section.

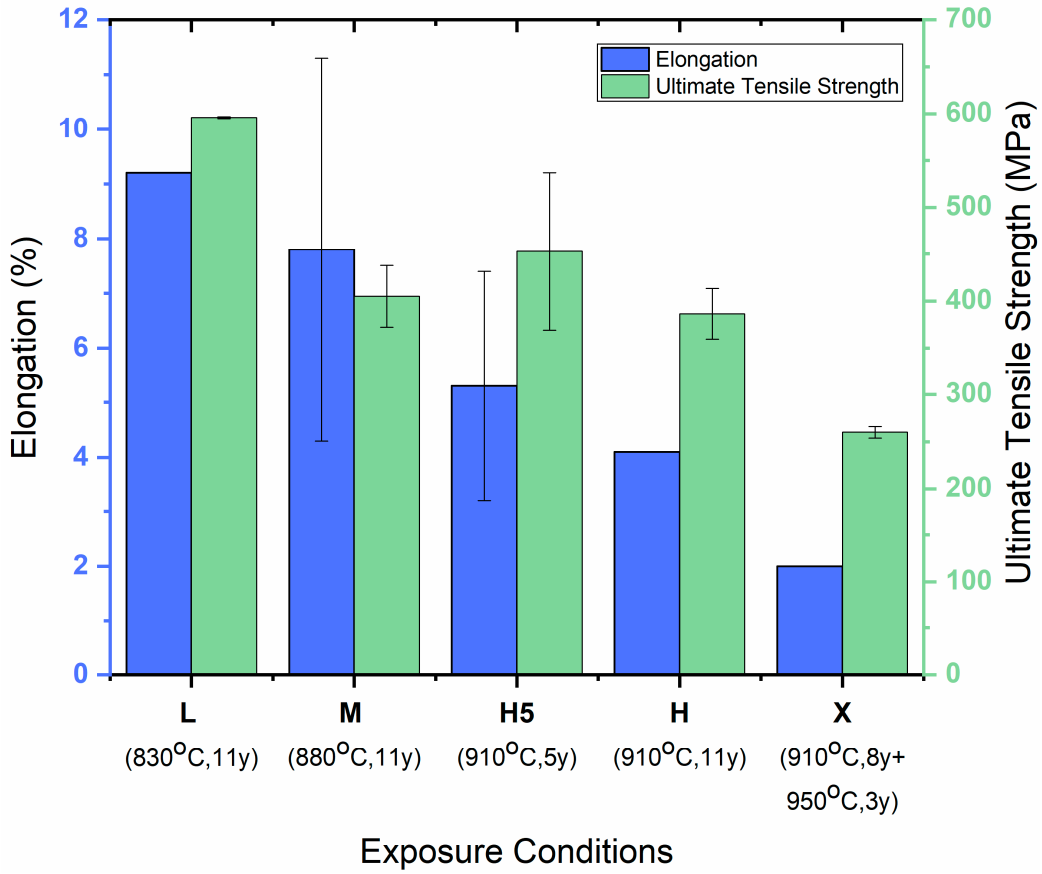

Figure 1. Room-temperature tensile properties vs. creep exposure conditions.

3.2. Microstructure Analysis

Carbides and other phases have been identified in this work with SEM/EDX analysis. Carbides were identified by the M:C ratio and the G-phase by the Ni:Nb:Si ratio. It should be noted that the EDX composition analysis of carbides is semi-quantitative, since it depends on the spot size relative to the carbide size. In order to avoid matrix contribution to the EDX spectrum, a low voltage was used during the EDX analysis. The analysis, therefore, provides a valid indication of the nature of the carbides.

The microstructure of the alloy consists of an austenitic matrix, forming dendrites, and a network of primary carbides. The dendrite length varies from 0.3 to 6.5 mm with an average length of 1.4 mm as depicted in Figure 2. The dendrites are oriented in the radial direction from the inner diameter (ID) to the outer diameter (OD) of the tube. Some dendrites are very long with a length being a significant

fraction of the tube thickness. In the as-cast condition, the austenite matrix is free of precipitates, as reported by Alvino et al. [6].

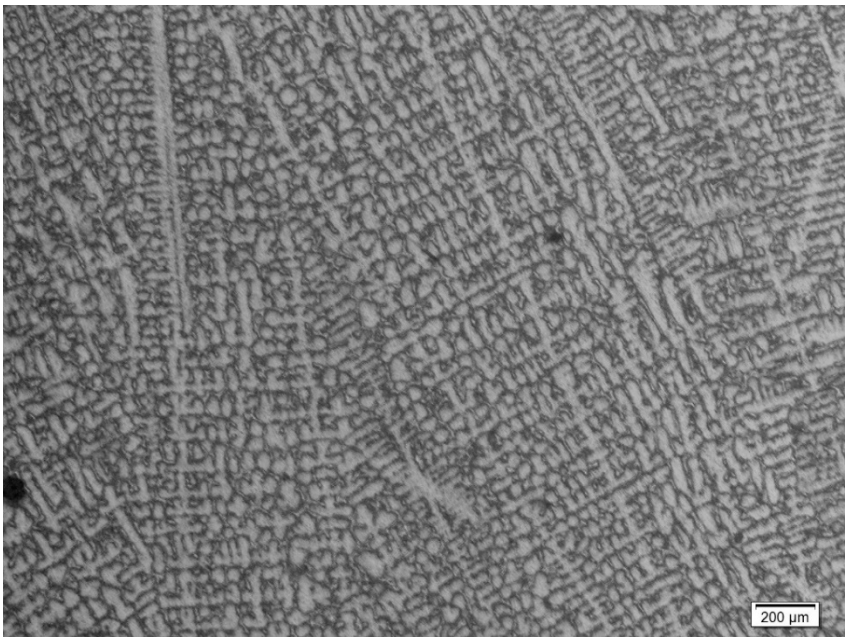

Figure 2. Microstructure of HP-Nb steel with austenite dendritic structure and carbide network in the interdendritic regions.

The carbides are located either in interdendritic or intradendritic regions and are either Cr-rich of M_7C_3 or $M_{23}C_6$ type and Nb-rich MC carbides. $M_{23}C_6$ are mostly grain boundary film-like carbides. M_7C_3 carbides exhibit a "Chinese script" morphology. Long-term exposure resulted in aging, manifested by the secondary precipitation in the austenitic matrix and coarsening of carbides. Such intragranular precipitation and carbide coarsening have also been observed by Attarian et al. [4] in HP-Nb steel after aging at 982 °C for 100 h. The results are presented for each exposure condition below.

Condition L (830 °C/11y): The microstructure is depicted in Figure 3a, consisting of M_7C_3 carbides. Identification of M_7C_3 carbides was based on SEM/EDX analysis of Figure 4. The numbers in Figure 4 correspond to EDX composition analysis, which is presented in Table 2. These carbides exhibit a "Chinese script" morphology. In addition to this morphology, M_7C_3 carbides appear with a needle morphology (Figures 3a and 4b).

Condition M (880 °C/11y): The microstructure is depicted in Figure 3b. The "Chinese script" morphology of M_7C_3 carbides is preserved with considerable rounding of edges. However, the needle-shaped M_7C_3 carbides have undergone a morphological transformation and exhibit a globular shape. This morphological transformation has been observed in directionally solidified HP-Ni steel [4]. The NbC carbides, originally present in the as-cast microstructure, transformed to a Ni-Nb silicide, the G-phase, with nominal composition $Ni_{16}Nb_7Si_6$, as depicted in Figure 5a,b. The numbers in Figure 5 correspond to EDX composition analysis, which is presented in Table 2. This transformation has been observed, in Ti-free alloys, by Pan [11] and by Soares et al. [17]. The G-phase is hard and brittle and, therefore, prone to cavity formation when the material is subjected to temperature excursions [11,17]. However, it should be noted that no cavities formed on the G-phase were detected at this operating condition. In addition, no $M_{23}C_6$ carbides were detected in condition M, indicating that the transformation of M_7C_3 to $M_{23}C_6$ carbides had not taken place.

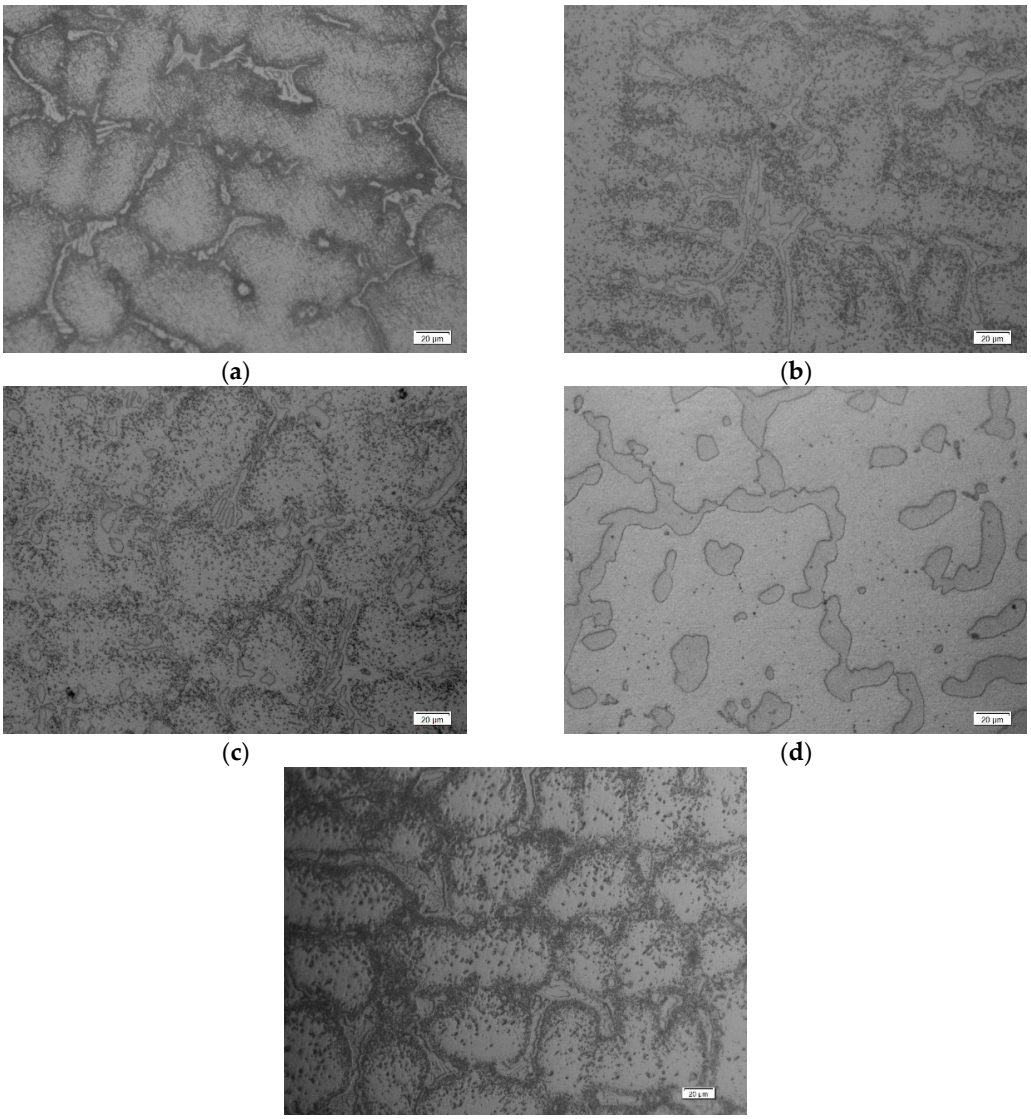

Figure 3. Microstructure revealed by metallography: (**a**) Condition L, (**b**) condition M, (**c**) condition H, (**d**) condition X, and (**e**) condition H5.

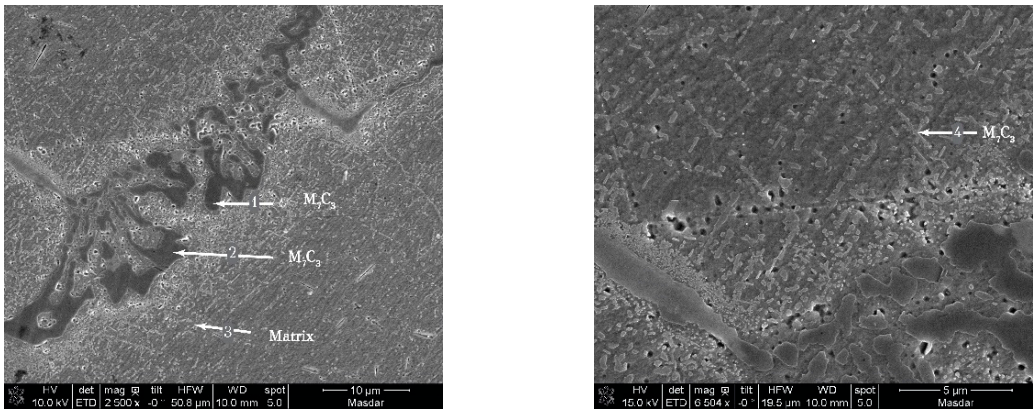

Figure 4. SEM image depicting M_7C_3 carbides in condition L. (**a**) "Chinese script" morphology; (**b**) needle morphology. Numbers indicate EDX composition analysis in Table 2.

Table 2. EDX analysis (at%).

Conditions		Cr	Ni	Fe	Nb	Ti	Si	C	M	M:C	Phases
Figure 4 (L)	1	54.3	4	10	-	-	-	31.6	68.3	2.16	M_7C_3
	2	55.8	4	8.5	-	-	-	31.6	68.3	2.16	M_7C_3
	3 matrix	23.8	29.6	38.5	0.3	0.5	-	4	-	-	-
	4 needles	19.4	21.5	22.2	-	-	-	31.8	63.1	1.98	M_7C_3
Figure 5 (M)	1	62.7	3.72	7.2	-	-	-	25.4	73.62	2.87	M_7C_3
	2	-	46	-	16.4	-	21.8	-	-	-	G
	3	-	54.17	-	19.1	-	26.7	-	-	-	G
	4	59.2	3	6	-	-	-	32	68.2	2.13	M_7C_3
	5	-	55	-	19.6	-	26	-	-	-	G
Figure 6 (H)	1	68	4	7	-	-	-	21	79	3.76	$M_{23}C_6$
	2	67.5	3.8	5.5	-	-	-	23.3	76.8	3.30	$M_{23}C_6$
	3	67.15	4.2	5.9	-	-	-	22.8	77.25	3.38	$M_{23}C_6$
	4	67.1	4.3	5.8	-	-	-	22.7	77.2	3.4	$M_{23}C_6$
Figure 7 (X)	1	59	3	11	5	-	-	22	78	3.54	$M_{23}C_6$
	2	59.2	3.7	10	4.3	-	-	22.6	77.2	3.41	$M_{23}C_6$
	3	46.7	20.1	3.9	4.6	-	-	21.5	75.3	3.50	$M_{23}C_6$
Figure 8a (H5)	1	-	-	-	52.2	1.7	-	46.1	53.9	1.17	MC
	2	-	-	-	50	2.7	-	47.3	52.7	1.11	MC
	3	-	-	-	51.3	2.5	-	46.2	53.8	1.16	MC
	4	-	-	-	41.4	5	-	53.6	46.4	0.86	MC
	5	53.4	7.8	16.8	-	-	-	22	78	3.54	$M_{23}C_6$
	6	59	4.7	15.3	-	-	-	21	79	3.76	$M_{23}C_6$
	matrix	25.4	33.4	34.7	-	-	-	5.2	-	-	-
	matrix	25.9	33.2	34.6	-	-	-	5	-	-	-
Figure 8c (H5)	1	57.4	1.4	7.6	-	-	-	33.6	66.4	1.97	M_7C_3
	2	28.1	22.2	29.2	-	-	-	20.5	79.5	3.87	$M_{23}C_6$
	3	33.1	19.6	25.3	-	-	-	21.3	78	3.66	$M_{23}C_6$
	4	-	-	-	41.3	2.7	-	56	44	0.78	MC

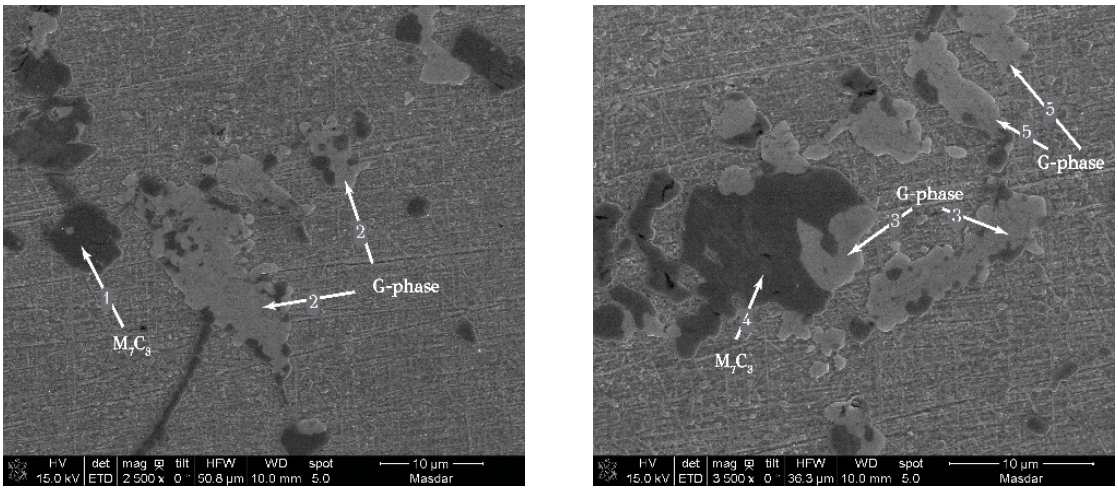

(**a**) (**b**)

Figure 5. SEM images, (**a**,**b**), depicting M_7C_3 carbides and G-phase in condition M. Numbers indicate EDX composition analysis in Table 2.

Condition H (910 °C/11y): The microstructure is depicted in Figure 3c. Most of the M_7C_3 carbides have transformed into the more stable $M_{23}C_6$ carbides as shown in Figure 6a,b. The numbers in Figure 6 correspond to EDX composition analysis, which is presented in Table 2. Significant coarsening of the $M_{23}C_6$ carbides has also taken place driven by the reduction in interfacial energy.

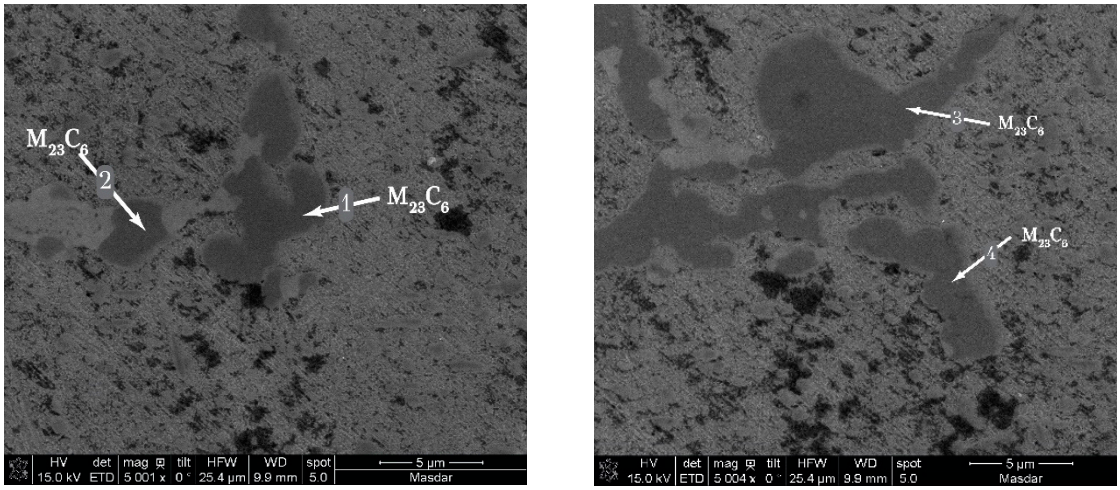

(**a**) (**b**)

Figure 6. SEM images, (**a**,**b**), depicting $M_{23}C_6$ carbides in condition H. Numbers indicate EDX composition analysis in Table 2.

Condition X (910 °C/8y + 950 °C/3y): The microstructure is depicted in Figure 3d. All carbides are of the $M_{23}C_6$ type and significant coarsening has taken place due to exposure at high temperature (950 °C). Nb has also been incorporated in the $M_{23}C_6$ carbides as indicated in Figure 7a,b. The numbers in Figure 7 correspond to EDX composition analysis, which is presented in Table 2.

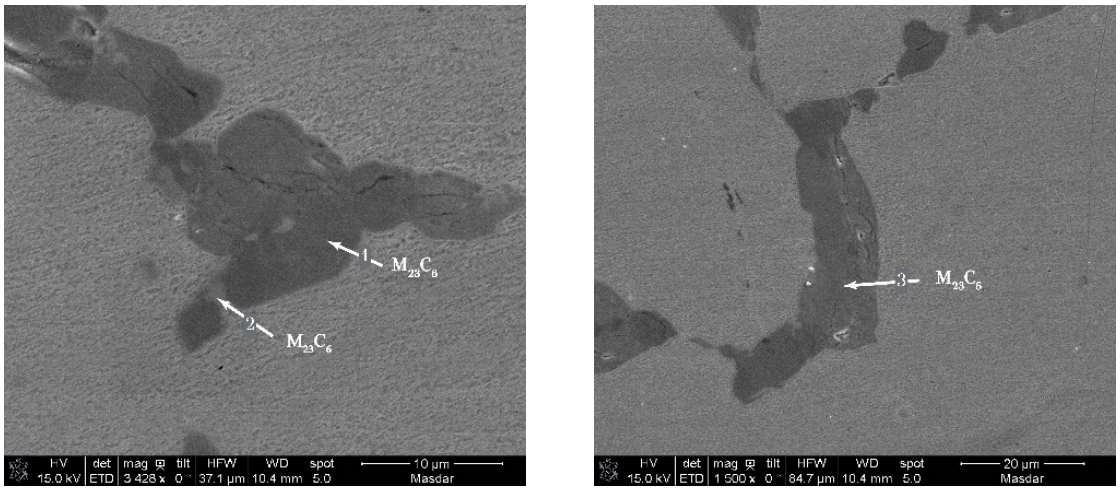

(**a**) (**b**)

Figure 7. SEM images, (**a**,**b**), depicting coarse $M_{23}C_6$ carbides in condition X. Numbers indicate EDX composition analysis in Table 2.

Condition H5 (910 °C/5y): It is noted that the H5 condition concerns the material containing Ti. The optical micrograph of the microstructure is depicted in Figure 3e. The microstructure of H5 material was investigated with SEM operating in the SE and BSE modes. Typical microstructures are depicted in Figure 8. The numbers in Figure 8 correspond to EDX composition analysis, which is presented in Table 2. MC carbides (Nb-rich), appear white, while $M_{23}C_6$, Cr-rich carbides appear dark grey in the BSE images due to the difference in atomic number between Nb and Cr. SEM-BSE imaging has been used by other researchers for carbide identification in cast heat-resistant steels [6,15]. The results indicate that MC carbides contain Ti, which according to Swaminathan et al. [18], stabilizes the MC carbide against transformation to the G-phase. This explains the fact that no G-phase was detected in the H5 material. Most probably, the transformation of the primary M_7C_3 carbides to

$M_{23}C_6$ is partial, contrary to the H condition where the transformation was complete. This partial transformation is depicted in Figure 8c with the associated EDX analysis of carbides in Table 2.

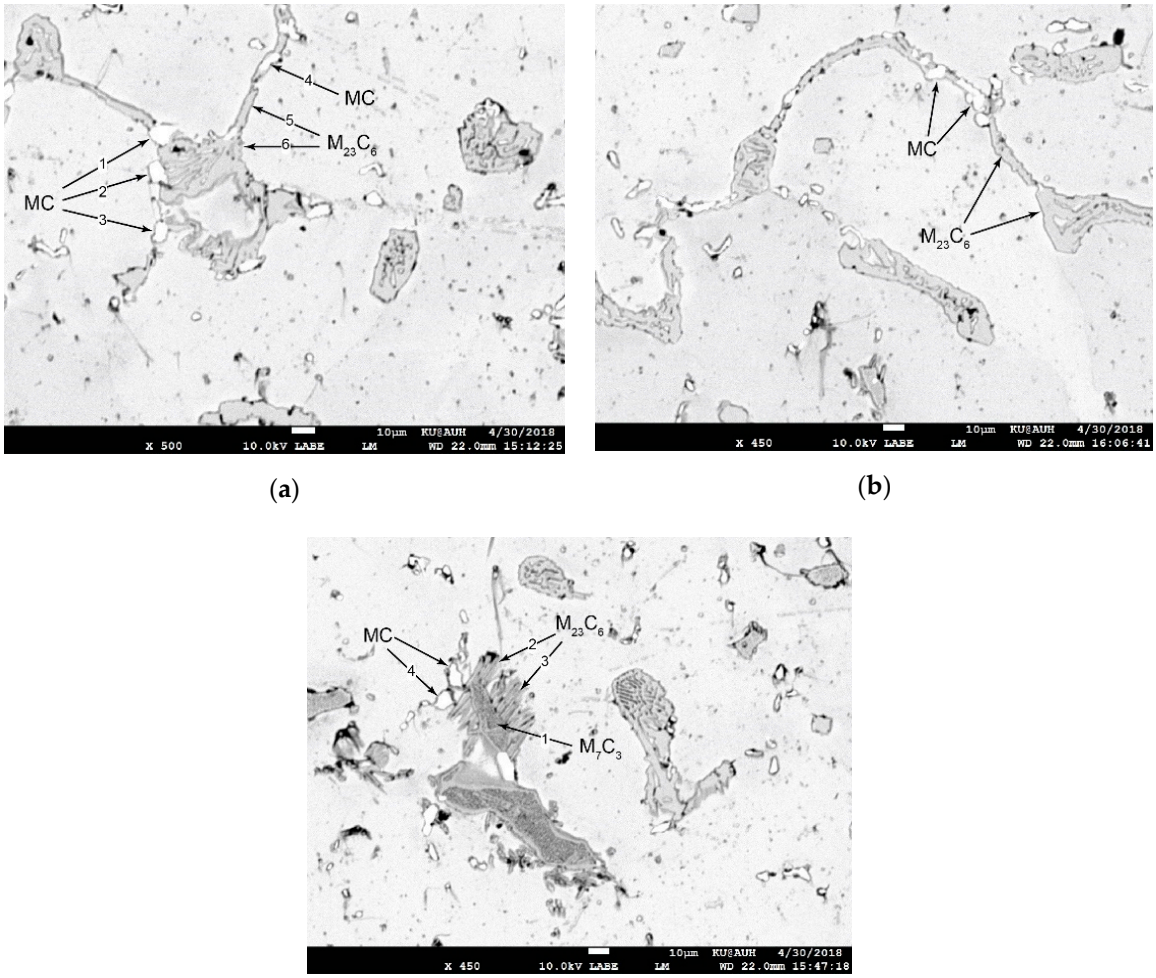

(**a**) (**b**)

(**c**)

Figure 8. SEM-BSE images depicting: (**a**,**b**) MC and $M_{23}C_6$ carbides in condition H5; (**c**) transformation of M_7C_3 to $M_{23}C_6$ carbide after creep exposure of 5 years. Numbers correspond to EDX composition analysis in Table 2.

4. Discussion

Creep resistance in cast steel reformer tubes depends, among other factors, on the thermal stability of the carbides. During operation at high temperatures, the carbides undergo phase changes as well as morphological changes, which degrade the creep resistance of the material. Phase changes involve the transformation of primary M_7C_3 to the more thermodynamically stable, at those temperatures of operation, $M_{23}C_6$. Morphological changes involve the coarsening of carbides driven by the reduction of interfacial energy [4,6]. Finally, an aging reaction, manifested as secondary precipitation of carbides within the austenitic matrix takes place during creep exposure [6]. In the present work, the transformation of M_7C_3 to the more stable $M_{23}C_6$ was observed to take place only at 910 °C and above for 11 years of operation period (conditions H and X). In these conditions the transformation is complete. In an intermediate operation period of five years (condition H5), the M_7C_3 to $M_{23}C_6$ transformation is partial. Significant coarsening of the carbides takes place at high temperatures (conditions H and X) while at lower temperatures the changes are morphological, i.e., the rounding of edges or the change from needle-shaped carbides to a globular morphology (condition M). Another interesting aging phenomenon during creep exposure is the transformation of the primary MC carbides

to the Ni-Nb silicide of G-phase manifested at intermediate temperatures (condition M). At higher temperatures, the G-phase dissolves and the Nb is incorporated in the $M_{23}C_6$ carbide. Similar observations regarding the type and morphologies of various carbides in creep-exposed HP-Nb steels have been reported by Allesio et al. [2] and Almeida et al. [15]. Finally, the presence of NbC carbides and the corresponding absence of G-phase in the H5 condition in the Ti-containing material validated previous observations that Ti stabilizes the MC carbide and acts against the transformation of the MC carbides to the G-phase [11,17]. As a result of aging the room temperature tensile elongation (strain to failure) is reduced considerably. The reduction is higher the higher the temperature of exposure. This reduced ductility makes the material prone to cracking due to expansions and contractions, which take place during shut-down/start-up of the reformer furnace.

5. Conclusions

An investigation of aging phenomena during creep has been conducted for HP-Nb cast reformer tubes. Based on the results presented above, the following conclusions can be drawn:

Aging was manifested by carbide precipitation, carbide coarsening and transformation from M_7C_3 to $M_{23}C_6$ carbides.

The MC carbides transform to the G-phase during creep exposure making the material more prone to cavity formation. The presence of Ti in the steel of condition H5 prevented the transformation of MC carbides to the G-phase.

Morphological changes occur as needle to globular transitions, rounding of edges, and carbide coarsening take place during creep exposure.

As a result of aging phenomena, the room-temperature tensile ductility is reduced, making the material prone to cracking during shut-down/start-up operations.

Author Contributions: Conceptualization, G.N.H.; methodology, K.P.; mechanical testing H.K. and A.D.Z.; metallography S.I.A., P.C., H.M. and S.J.; SEM/EDX, K.P.; paper preparation and editing, G.N.H.

Funding: This research received no external funding.

Acknowledgments: The assistance of Roba Khaled Saab of KU with SEM/EDX is greatly appreciated.

Conflicts of Interest: The authors declare no conflict of interest.

References

1. Barbabela, G.D.; de Almeida, L.H.; da Silveira, T.L.; Le May, I. Role of Nb in modifying the microstructure of heat-resistant cast HP steel. *Mater. Charact.* **1991**, *26*, 193–197. [CrossRef]
2. Alessio, D.; Gonzalez, G.; Pirrone, V.F.; Iurman, L.; Moro, L. Variation of Creep Properties in HP Steel by Influence of Temperature. *Proc. Mater. Sci.* **2012**, *1*, 104–109. [CrossRef]
3. API. *Calculation of Heater Tube Thickness in Petroleum Refineries: API Recommended Practice 530*, 3rd ed.; API: Washington, DC, USA, 1988.
4. Attarian, M.; Taheri, A.K. Microstructural evolution in creep aged of directionally solidified heat resistant HP-Nb steel alloyed with tungsten and nitrogen. *Mater. Sci. Eng. A* **2016**, *659*, 104–118. [CrossRef]
5. Ray, A.K.; Roy, N.; Raj, A.; Roy, B.N. Structural integrity of service exposed primary reformer tube in a petrochemical industry. *Int. J. Pres. Ves. Pip.* **2016**, *137*, 46–57. [CrossRef]
6. Alvino, A.; Lega, D.; Giacobbe, F.; Mazzocchi, V.; Rinaldi, A. Damage characterization in two reformer heater tubes after nearly 10 years of service at different operative and maintenance conditions. *Eng. Fail. Anal.* **2010**, *17*, 1526–1541. [CrossRef]
7. Bonaccorsi, L.; Guglielmino, E.; Pino, R.; Servetto, C.; Sili, A. Damage analysis in Fe–Cr–Ni centrifugally cast alloy tubes for reforming furnaces. *Eng. Fail. Anal.* **2014**, *36*, 65–74. [CrossRef]
8. Gong, J.-M.; Tu, S.-T.; Yoon, K.-B. Damage assessment and maintenance strategy ofhydrogen reformer furnace tubes. *Eng. Fail. Anal.* **1999**, *6*, 143–153. [CrossRef]
9. Lee, J.H.; Yang, W.J.; Yoo, W.D.; Cho, K.S. Microstructural and mechanical property changes in HK40 reformer tubes after long term use. *Eng. Fail. Anal.* **2009**, *16*, 1883–1888. [CrossRef]

10. Ray, A.K.; Kumar, S.; Krishna, G.; Gunjan, M.; Goswami, B.; Bose, S.C. Microstructural studies and remnant life assessment of eleven years service exposed reformer tube. *Mater. Sci. Eng. A* **2011**, *529*, 102–112. [CrossRef]
11. Pan, J.-H.; Chen, Z.; Fan, Z.-C.; Wu, Y.-C. An experimental investigation on manifold failure and material deterioration. *Int. J. Pres. Ves. Pip.* **2018**, *162*, 1–10. [CrossRef]
12. Ray, A.K.; Sinha, S.K.; Tiwari, Y.N.; Swaminathan, J.; Das, G.; Chaudhuri, S.; Singh, R. Analysis of failed reformer tubes. *Eng. Fail. Anal.* **2003**, *10*, 351–362. [CrossRef]
13. Monobe, L.S.; Schön, C.G. Characterization of the cold ductility degradation after aging in centrifugally cast 20Cr32Ni+Nb alloy tube. *Int. J. Pres. Ves. Pip.* **2009**, *86*, 207–210. [CrossRef]
14. Kenik, E.A.; Maziasz, P.J.; Swindeman, R.W.; Cervenka, J.; May, D. Structure and phase stability in a cast modified-HP austenite after long-term ageing. *Scr. Mater.* **2003**, *49*, 117–122. [CrossRef]
15. De Almeida, L.H.; Ribeiro, A.F.; Le May, I. Microstructural characterization of modified 25Cr–35Ni centrifugally cast steel furnace tubes. *Mater. Charact.* **2002**, *49*, 219–229. [CrossRef]
16. *ISO 6892-1:2016. Metallic Materials—Tensile testing—Part 1: Method of Test at Room*; International Organization for Standardization: Geneva, Switzerland, 2016.
17. De Almeida Soares, G.D.; de Almeida, L.H.; da Silveira, T.L.; Le May, I. Niobium additions in HP heat-resistant cast stainless steels. *Mater. Charact.* **1992**, *29*, 387–396. [CrossRef]
18. Swaminathan, J.; Guguloth, K.; Gunjan, M.; Roy, P.; Ghosh, R. Failure analysis and remaining life assessment of service exposed primary reformer heater tubes. *Eng. Fail. Anal.* **2008**, *15*, 311–331. [CrossRef]

© 2019 by the authors. Licensee MDPI, Basel, Switzerland. This article is an open access article distributed under the terms and conditions of the Creative Commons Attribution (CC BY) license (http://creativecommons.org/licenses/by/4.0/).